

HSM2023-00005

THE EFFECT OF BROACHING TOOL CUTTING EDGES POLISHING ON PROCESS FORCES AND TEMPERATURE

C. Pérez-Salinas^{1,2*}, LN. López de Lacalle^{1,3}, P. Fernández-Lucio², G. Gómez-Escudero², A. Del Olmo³

¹Universidad Técnica de Ambato, Faculty of Civil and Mechanical Engineering, Ambato, Ecuador

²University of the Basque Country (UPV/EHU), Dpt. of Mechanical Engineering, Bilbao, Spain

³Advanced Manufacturing Centre for Aeronautics (CFAA), University of the Basque Country, Zamudio, Spain

*Corresponding author; e-mail: cf.perez@uta.edu.ec

Abstract

In the industrial field, the search for improving the performance of machining tools considering their geometry, manufacturing, material, and coatings is a priority. This research focuses on optimizing the cutting edge for broaching Inconel 718. Drag-finishing was used to round and polish the cutting edge of a K10-Co 7% grade tungsten carbide roughing tool. The results reveal that increasing the cutting-edge radius affects the process forces increasingly, especially the thrust force. From the minimum tested radius of 5 micrometers to the maximum radius of 35 micrometers, the cutting and thrust force doubles at uncut thicknesses (*RPT*) of 75 and 100 micrometers. The plowing force is hardly affected. The shear coefficient *K_{cc}* also shows growth as the radius of the cutting-edge increases. The temperature increases proportionally with the radius, and in addition, the simulations show a change of the temperature distribution in the cutting profile with the change of the cutting-edge radius. Thus, the preparation of the cutting-edge could be crucial in the performance of the broaching process.

Keywords:

Broaching process, Process forces, Plowing force, Cutting-edge, Rounding, Polishing, Brushing

1 INTRODUCTION

In recent years Inconel 718 has been a challenging engineering material due to its broad utility, superior mechanical performance, high wear resistance at high temperatures and complex machinability [Klocke et al., 2013; Engine materials | MTU Aeroreport]. Inconel 718 is known as a difficult material to machining due to its low thermal conductivity and its tendency to surface harden by deformation when the cutting tool passes through it [Bouzakis et al., 2014a; Klocke et al., 2013]. Adhesive wear tends to appear on the cutting edge and this, in addition to the above, will affect tool life. At an industrial level, one of the important variables in machining is the resulting cutting forces and temperature [del Olmo et al., 2022]. Knowing the behaviour of these variables in the machining of engineering materials is imperative in the reliable control of the process, as well as in the design of tools.

In important fields such as aeronautics, automotive, nuclear, Inconel 718 broaching is used in the manufacture of elements where precision and quality are critical. To meet the demands of precision and quality, manufacturers and researchers have led to the study of the micro geometry of cutting tools to improve their performance.

Broaching tool are the cutting tools of the broaching process that have a wide range of simple and special

shapes depending on the products to be machined. In the aeronautical industry Broaching tool remain the ideal choice for machining turbine discs in aircraft engines. The surface quality and accuracy meet the requirements of this industry [Fabre et al., 2017]. The "firtree" are special grooves for the coupling of the blades on the turbine disk, so the surface must be of high quality and accuracy. Rectangular shaped Broaching tool are used for the roughing process, while finishing Broaching tool are fir tree shaped to achieve the *firtree* on the Inconel 718 disk (Fig.1).

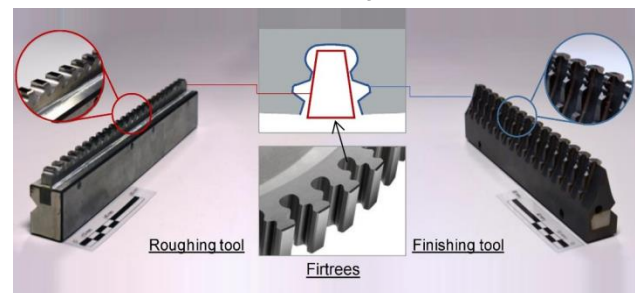


Fig. 1: External broaching tools for turbine disks

In the roughing process, a greater amount of material is removed, therefore, roughing Broaching tool tend to wear faster and can affect the machined surface [Sajeev et al.,

2012b, 2012a]. Hence the importance of studying the cutting conditions to improve their performance and reduce the effect on cutting quality.

Several studies have focused on the preparation of cutting edges (rounding of the cutting edge, r_e) and its influence on cutting forces and temperature [Pérez-Salinas et al., 2022; Lv et al., 2022; Cortés, 2009]. In addition, it has been found that in several materials the positive influence of rounding defined as: increase in service life, reduction of cracks in the material, mechanical strength at the cutting edge and changes in the behavior of cutting forces.

In broaching, considered as a process very close to orthogonal cutting. In orthogonal cutting, the forces F_x , F_y acquired in the cutting process by means of a dynamometer include the forces acting on the tool-work piece interaction. According to the approach of [Albrecht, 1960], in a tool with a rounded cutting edge, the process forces (Fig. 4) are those acting on the cutting surface, the cutting edge and the incident surface of the tool. During the machining process, the release of material from the workpiece occurs at the same time as a plowing process takes place. The driving force that allows the material to be removed and the chip to form is the force acting on the cutting face (F_a). The plowing force (F_p), on the other hand, is the resultant of the pressure exerted on the rounded edge and flank of the tool. The distinction and evaluation of these forces allows us to understand the phenomenon of wear, surface effects such as roughness and residual stresses caused by the machining of the material.

Machining simulations have allowed the extension of cutting studies, as well as helping to understand the progress of difficult to monitor or measure variables such as temperature. In the broaching process, studies have been carried out on the behavior of cutting forces and temperature as the angle of attack and different cutting speeds change [Zhang and Chen, 2012]. However, how the cutting-edge radius affects these variables has not been studied.

In this work, four variations of initial broaching radius and four different values of rise per tooth (RPT) were employed. The objective was to analyze their impacts on cutting forces, temperature and their effects on the Inconel 718 broaching process, improving our understanding of cutting performance, tool wear and surface effects on the workpiece.

2 METHODOLOGY

2.1 Cutting-edge preparation and characterization

The cut edges were prepared with radius r_e between 5 to 35mm. The rounding of the edges was generated by Drag-finishing process [Pérez-Salinas et al., 2022]. The drag-finishing process is a surface finishing method that involves the controlled dragging of parts through an abrasive medium or polishing compound. Used to round edges, remove burrs, and improve surface quality, this process employs vibration and dragging in a rotating drum or bowl to achieve an improvement in the geometry and texture of machined parts.

For the characterization of the rounding of the cutting edge, the method proposed by [Denkena et al., 2013]. For this purpose, an *Alicona InfiniteFocus* device was used as a measuring instrument.

2.2 Experimental procedures

The broaching experiments were implemented in dry conditions as shown in Fig. 2. An aged Inconel 718 (Hardness of 45 HRC) disc of diameter 100 mm was mounted on a *CMZ-TC25* turning center capable of withstanding 5000 N in its three axes, to allow a cutting length of 30 mm. The excellent rigidity properties of the machine due to its robustness allowed vibrations to be minimized. The machine's feed movements (0-30 m/min) limit the cutting speeds for the application of the broaching process.

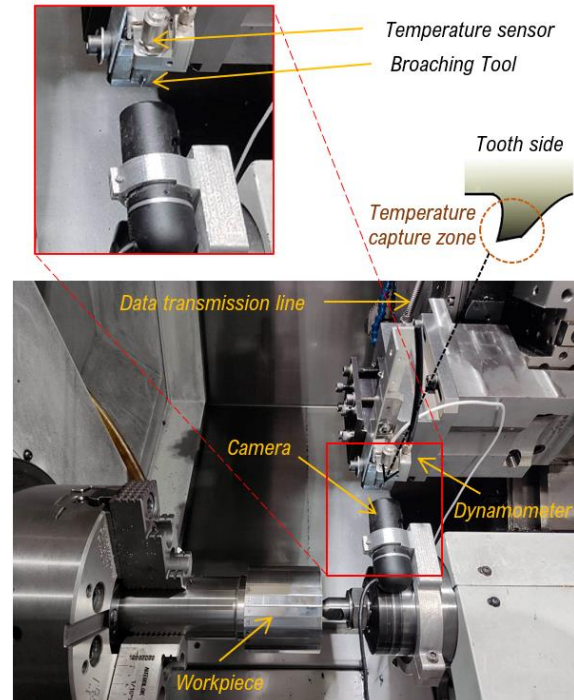


Fig. 2: Experimental set-up for orthogonal cutting tests by broaching with one cutting-edge

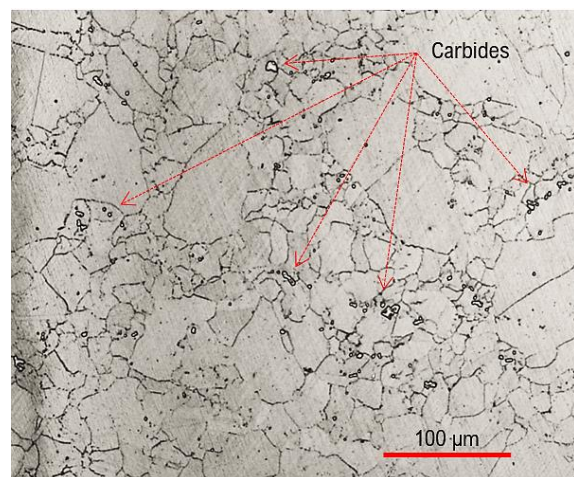


Fig. 3: Microstructure of the bars of Inconel 718

The tool was an uncoated Tungsten Carbide rectangular roughing broach segment (1 tooth) with 6%Co with a cutting width of 8 mm. Tab. 1 summarizes the tool geometry and cutting parameters used in the cutting tests. An *OPTRIS-CT-2M* infrared thermal camera with a resolution to monitor the temperature in the tool of 1 ms was used. The capture of the temperature on the tool was the lateral area of the cutting edge (Fig. 2). The cutting forces were measured

with the Kistler force dynamometer under orthogonal cutting conditions (measuring range ± 10 kN in the z-axis and ± 5 kN in the x and y directions). Two repetitions were performed for each broaching condition. Further details are presented in Tab. 1.

Tab. 1: Cutting parameters and tool geometries

Parameter	Unit	Value
Cutting speed, V_c	(m/min)	20
Rake angle, γ	($^\circ$)	7
Clearance angle, α	($^\circ$)	3
cutting width, B	(mm)	8
Rise per tooth, RPT	(μm)	25, 50, 75, 100
Radius edge, r_e	(μm)	5, 12, 25, 35

2.3 Simulation

The simulated thermal loads in the shear zone were approximated by the *Deform 2D* software package based on an implicit Lagrangian formulation. Both the thermal properties of cemented carbide and Inconel 718 were taken from the *Deform 2D* library.

The inverse method was used to determine the constitutive equation of Inconel 718. The constants A , B , C , m and n of the Johnson Cook equation (1) were identified as follows [Vogtel et al., 2013], as shown in Tab. 2.

$$\sigma_{yld} = [A + B \cdot \epsilon^n] \cdot \left[1 + \ln\left(\frac{\dot{\epsilon}}{\dot{\epsilon}_0}\right)\right] \cdot \left[1 - \left(\frac{T - T_0}{T_{melt} - T_0}\right)^m\right] \quad (1)$$

Tab. 2: Constants of the Johnson cook equation

A (MPa)	B (MPa)	C	n	m
851.6655	657.6151	0.0105	0.2280	3.1169

2.4 Methodology to reveal the plowing force

For the determination of the chip-forming forces F_h , and the plowing force F_p , from these data can be determined by the same approach given by [Albrecht, 1960]. The approach is based on the assumption that (1) the total force in a cutting process increases linearly with increasing feed, provided that the area of the cutting edge, which is influenced by the plowing force, is fully engaged, (2) the plowing force F_p changes with increasing feed, and (3) the coefficient of friction μ at the tool-chip interface is independent of the thickness of the uncut chip. The force values can be extrapolated to an uncut chip thickness of $t = 0$. The resulting force is the plowing force F_p (Fig. 3). Furthermore, the direction of the axes acting on the orthogonal cut for the present test at the turning centre F_z and F_x correspond to the direction of the horizontal component of the chip removal force and the vertical component of the ploughing force respectively.

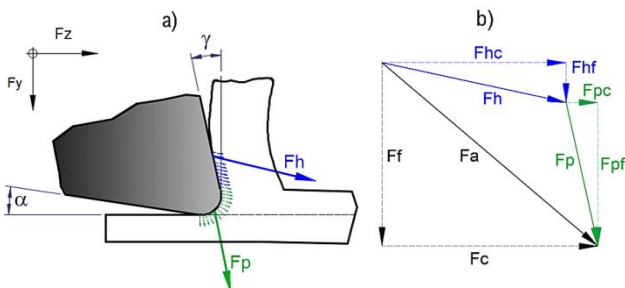


Fig. 4: Influence of the cutting-edge radius on the machining, a) Acting forces: plowing force F_p and chip forming force F_h , b) Decomposition of active or result force

The net cutting force F_{hc} and the thrust force F_{hf} for chip formation can be represented by equations (2) and (3):

$$F_{hc} = F_c - F_{pc} \quad (2)$$

$$F_{hf} = F_f - F_{pf} \quad (3)$$

Knowing the plowing and thrust forces, the average coefficients of friction μ at the tool-chip interface on the rake face can be determined by equation (4):

$$\mu = \frac{\sin\gamma \cdot F_{hc} + \cos\gamma \cdot F_{hf}}{\cos\gamma \cdot F_{hc} - \sin\gamma \cdot F_{hf}} \quad (4)$$

2.5 Determination of shear coefficient

Altintas' mechanistic cutting model with two force components in the chip flow plane was used to determine the cutting coefficients (specific cutting force K_c and K_e respectively). This model considers edge-related forces and cutting effects. The edge effect corresponds to the forces produced by the friction between the flank surface and the workpiece and to the forces due to the edge radius. The cutting effect is produced by the flow of chips on the rake face (equation (5) and (6)). The coefficients are determined by experiments carried out during orthogonal cutting of the nickel-based superalloy.

$$F_c = K_{cc} \cdot b \cdot h + K_{ce} \cdot b \quad (5)$$

$$F_f = K_{fc} \cdot b \cdot h + K_{fe} \cdot b \quad (6)$$

3 RESULTS AND DISCUSSION

3.1 Edge polishing

Fig. 5 and Tab. 3 shows the results of the characterization of the cutting-edge preparation. In general, a symmetrical rounding tendency was obtained. This is evidenced by K values close to 1 (total symmetry).

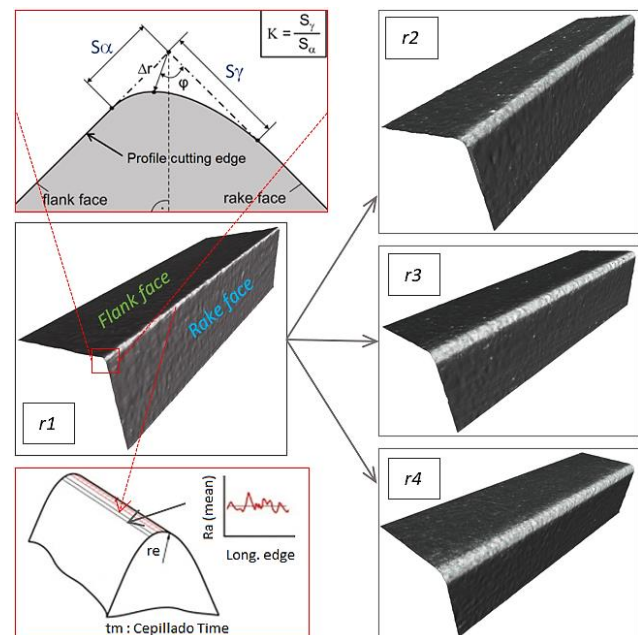


Fig. 5: Cutting-edge rounding characterization results

Tab. 3: Cutting-edge rounding characterization results

radius	Radius r_e [μm]	K	$T_m[s]**$	$Ra[\mu\text{m}]$
$r1^*$	5	1.45	0	0.350
$r2$	12	1.31	82	0.307
$r3$	25	1.03	240	0.241
$r4$	35	1.18	300	0.235

* Original radius

** Edge preparation time by Drag finishing

The original manufacturing rounding was approximately 5 micrometers, which is before cutting-edge polishing. After a preparation time of t_m , edge radius of 15 μm , 25 μm and 35 μm was achieved, which are within common ranges of broaching tool fabrication and good results found in previous work on machining Inconel 718 [Drozda et al., 1983; Zhang and Chen, 2012; Bouzakis et al., 2014b]. In addition to the above, it is evident that the longer the dragging time T_m , the greater the radius obtained. Conversely, the longer the preparation time, the lower the average roughness of the cut edge.

3.2 Effects on broaching process forces and temperature

Fig. 6 shows the results of the influence of the edge radius on the forces and temperature of the cutting process. There is a higher sensitivity of the tangential or shear force F_c to the change of the edge radius with respect to the thrust or feed force F_f (Fig. 6a, Fig. 6b). This sensitivity is evidenced by an increase in the forces with a linear trend. Furthermore, it can be noted that the incidence of the radius effect increases with increasing uncut height.

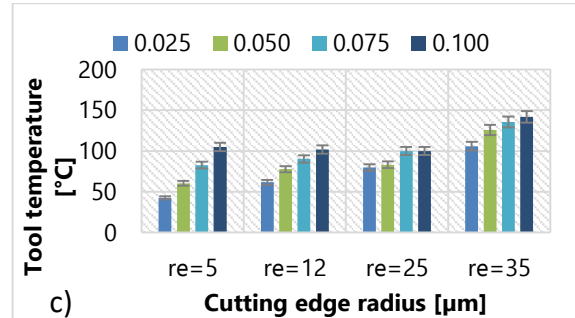
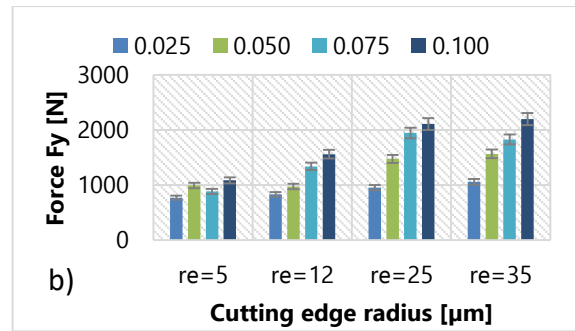
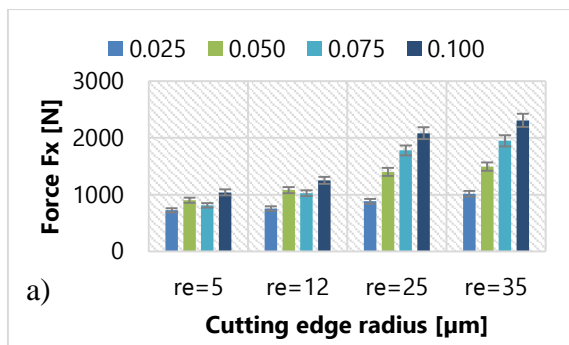


Fig. 6: Effect of cutting-edge radius on the broaching process, a) cutting force, b) feed force, c) temperature

The result of the temperature measurements of the cutting process can be seen in Fig. 6c. It is noted that the temperature is affected with increasing cutting-edge radius. For example, with RPT of 25 micrometers the sensed temperature increases by 100% when the cutting-edge radius is increased to 35 micrometers.

To better understand the effect of temperature on the shear zone, simulations of the same experimental shear conditions were performed using *Deform 2D* software. It was found that there is an influence of the radius on the temperature behavior. This effect is amplified when the shear rate is increased. Fig. 7 shows the effect of the four tested radii on the temperature in the shear process at a shear rate of 20 m/min. In all cases, the maximum temperature is located on the peeling face of the cutting plane. This is due, in principle, to the heat source originating from the cutting plane and is magnified due to the heat generated by friction on the rake face. It is observed that, when the radius is small (5 μm and 15 μm) the maximum

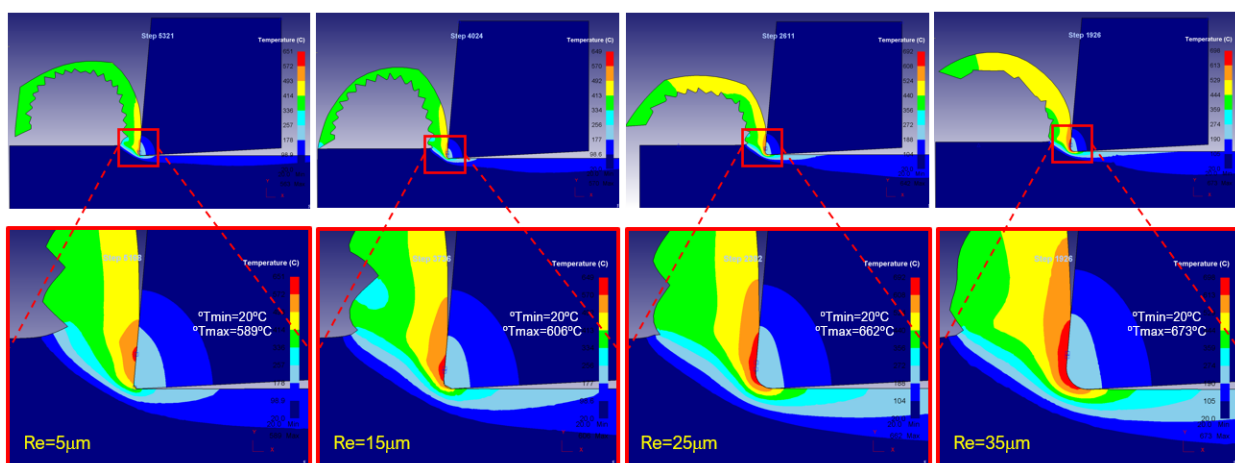


Fig. 7: Simulation of the effect of temperature on the cutting zone, under the conditions RPT=75 μm , $V_c=20\text{m/min}$, $\gamma=5^\circ$, $\alpha=3^\circ$

temperature is localized, whereas as the radius increases

the high temperatures are distributed both on the radius contour of the cutting edge and on the rake face. This is beneficial, since the wear would not be localized (e.g., crater wear) but progressive in the cutting profile, which would result in increased cutting-edge durability. Finally, the maximum temperature tends to decrease towards the rake face as the cutting-edge radius increases.

In the experimental cutting process, the force signals for all components showed particular characteristics (Fig. 8). Firstly, the shapes of the force spectra confirm the orthogonal cutting process carried out. That is to say, the spectra of the F_y and F_z components are characteristic of the machining process, except for the spectrum of the F_x component, where vibration is only evident when the cutting-edge passes through the material. On the other hand, the spectra of all the components show an initial peak of force that marks the initial impact of the introduction of the tool into the material, which then tends to stabilize. However, the loading signal of the cutting-edge with radius 25 showed a slight positive slope that starts at approximately the first third of the cutting length and ends with the exit of the tooth from the material. This may be a result of the increased flank wear and edge breakage that this cutting edge underwent in the previous cutting steps (Fig. 9). This is logical due to the difficult cutting of Inconel 718 in addition to the experiment in unlubricated conditions. This will be discussed in more detail in later work. The force curves obtained have the same characteristics as those found in the work by [Fabre et al., 2017], where the transitions of the curves related to the chip formation are identified and explained. Finally, the peak force at the tooth entry into the material in the thrust component F_y is lower than the peak force in the tangential component F_z , indicating that the tool suffers more impact energy frontally, i.e., perpendicular to the direction of cutting motion.

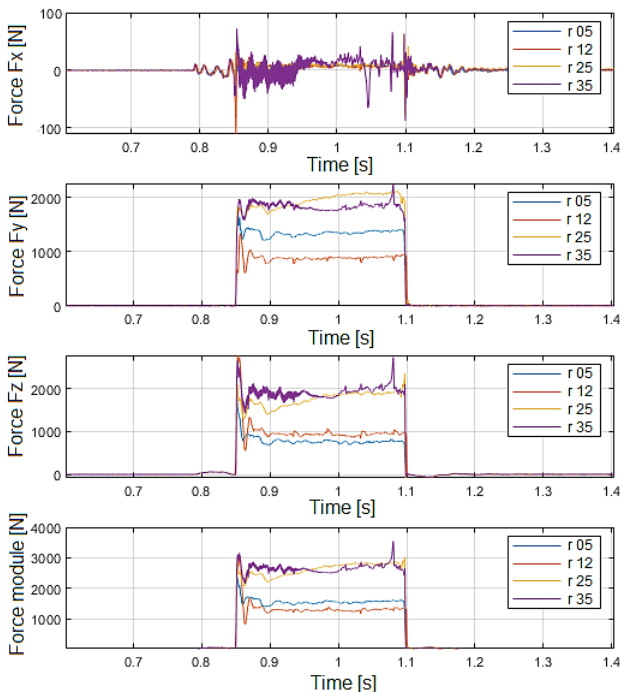


Fig. 8: Monitored forces of the orthogonal broaching process with $V_c=20$ m/min and $RPT=75\mu\text{m}$. Application of 400 Hz low pass filter.

The chips showed uniform curling and their diameter tended to increase as the RPT increased as shown in Fig. 10.

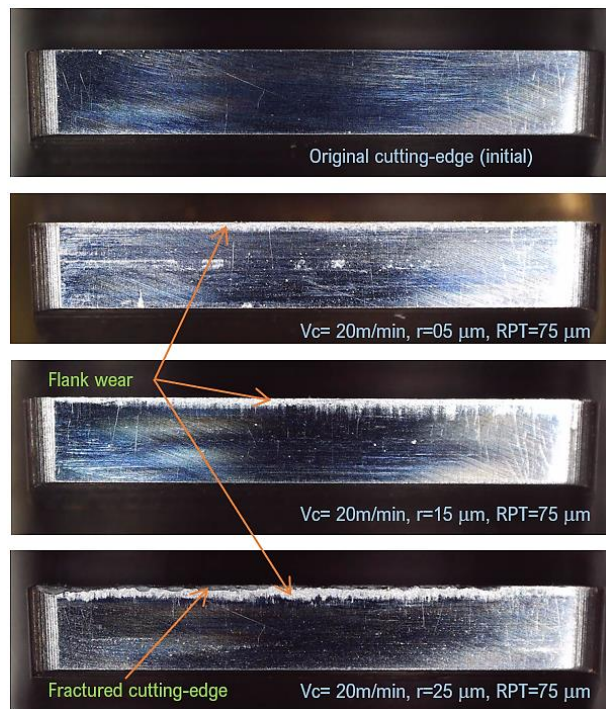


Fig. 9: Types of wear on the cutting edge after orthogonal broaching at different radius

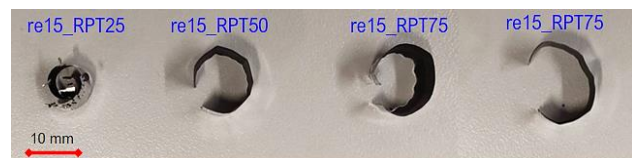


Fig. 10: Chip form obtained from the broaching process

In relation to the action of the cutting-edge radius on the machining performed, it is evident that the process forces increase as the cutting-edge radius increases. In the tests performed, a thrust force (F_y) is evident. The range of thrust forces is close to the range of tangential or shear forces (F_z). This behavior is different in comparison with other studies such as that of [Wyen and Wegener, 2010], where the values of F_y results low compared to F_z . Therefore, it is estimated that this high thrust force will influence the machined surface both in terms of surface quality and residual stresses. These effects will be further investigated and reported in subsequent works.

Fig. 11 shows the temperature spectrum captured from the experimental test. As an example, the effect of the radius of 12 μm at different RPT on the lateral temperature of the tool in the pick-up zone was taken (Fig. 2). The spectrum shows an increase in the instantaneous temperature, this lasts for about 300 ms at tool entry into the material and is maintained until half the cutting length (1000 ms). Then the temperature drops from 4 to 10 $^\circ\text{C}$ (depending on the RPT) gradually over a time of 700 ms, where it stabilizes until the exit of the tooth (350 ms). Finally, when the tool exits the material, the temperature decreases by convection cooling with the ambient air slowly until thermal equilibrium is reached. In the example shown, all the signals comply except for the signal corresponding to the rise per tooth 75 micrometers, where the chip sticks to the edge of the tool. On the other hand, it can be clearly noticed that the influence of the RPT on the temperature in the orthogonal broaching cutting process is greater than the influence of the radius (Fig. 6c), where the influence of the radius is

much smaller. It should be noted that, although the measured temperature is not in the chip-tool release surface interaction zone, the captured zone gives us a good appreciation of the temperature behavior in the different cutting conditions.

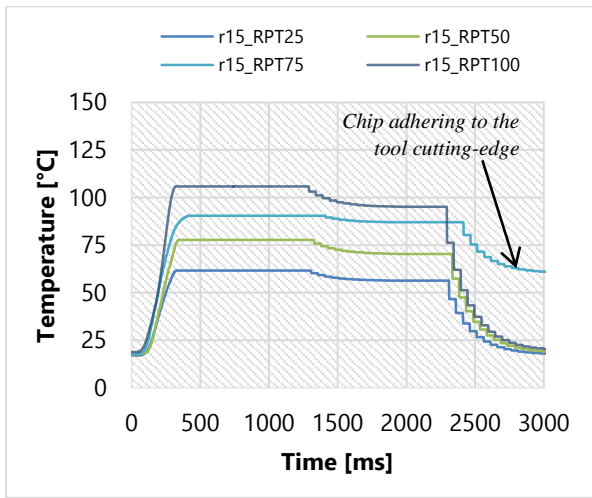


Fig. 11: Monitored temperatures of the orthogonal broaching process with $V_c=20$ m/min and radius= $15\mu\text{m}$

3.3 Specific shear force behavior

The specific cutting force behavior for the chip detachment effect and the specific cutting force due to the cutting-edge effect is shown in Fig. 12. K_c tends to grow as the cutting-edge radius increases, while K_e apparently tends to remain constant according to the Altintas model of orthogonal cutting. In the experiment, it is verified that the contribution of the edge to the shear of the material is limited, but still has some significance.

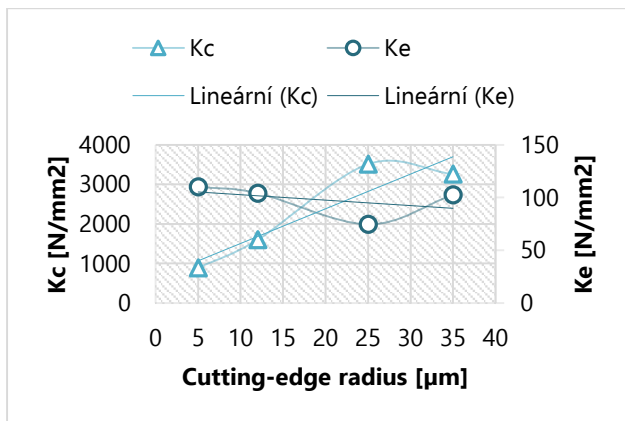


Fig. 12: Behavior of the specific cutting force to the change of the cutting-edge radius

3.4 Effect on plowing force

According to the approach of [Albrecht, 1960] the directions of the plowing forces F_p and the cutting force F_h can be found by plotting the forces measured in the experimental test versus various thicknesses of uncut chip h . For the case h corresponds to the rise per tooth. Fig. 13 shows the behavior of the average forces F_z and F_y found experimentally versus the rise per tooth. The results show the linear increase of the forces with increasing rise per tooth. For the present case of orthogonal broaching, the slopes of the fitted linear regression lines are similar for both shear and thrust forces [Guo and Chou, 2004]. In other

studies, the slope of the thrust force is smaller than the slope of the cutting force [Wyen and Wegener, 2010]. for orthogonal cutting by turning. This behavior could be due to the nature of the movement in the case of orthogonal broaching versus orthogonal turning, the different stiffness in the orthogonal axes, the asymmetry in cutting edge rounding (factor $K > 1$), flank wear, among other aspects, which should be studied in greater depth with a greater number of tests in different conditions.

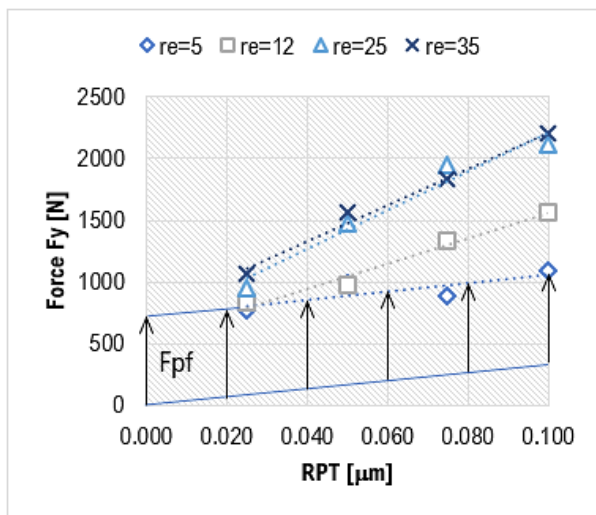
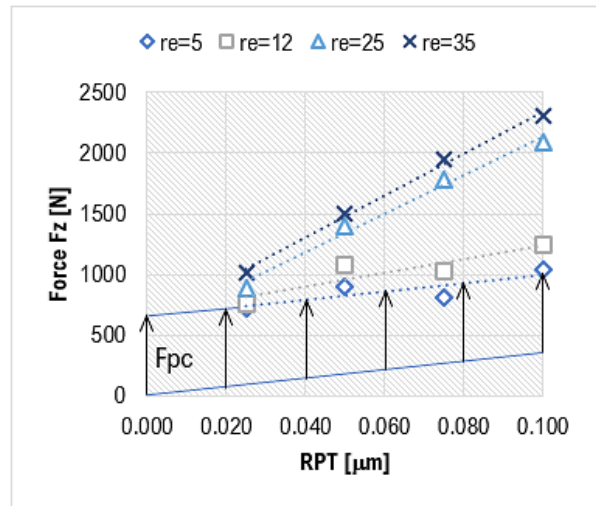


Fig. 13: Behavior of the average forces F_z and F_y versus different rise per tooth

Fig. 14 shows the results of the plowing force behavior for each cutting-edge radius at different rise per tooth. It can be noticed that the plowing force tends to be maintained both with changing radius and increasing RPT . This effect is best seen by taking the average value of the plowing force for each RPT that encompasses the plowing forces of each radius. Therefore, it can be said that the change in plowing force is not appreciable at change of radius and rise per tooth.

On the other hand, Fig. 15 shows the behavior of the chip formation force for each cutting-edge radius at different RPT . The result shows that for each condition (different cutting-edge radius at each RPT) the force increases gradually. This means that the tool in the cutting direction is subjected to higher cutting loads. Finally, unlike the plowing force, the chip forming force is influenced by both the cutting-edge radius and the RPT .

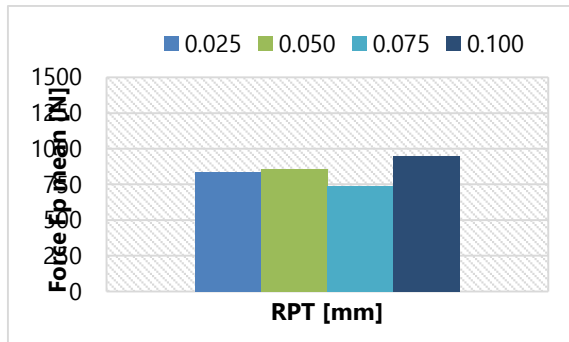
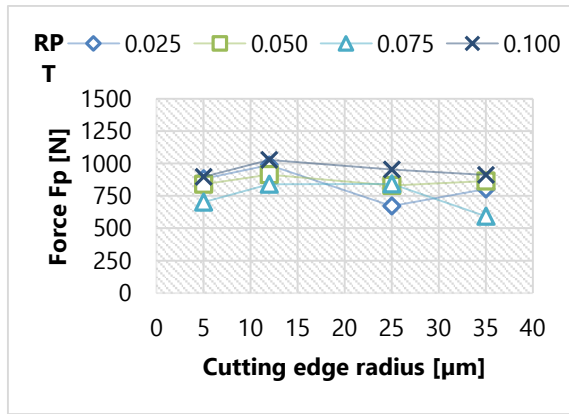


Fig. 14: Behavior of plowing force

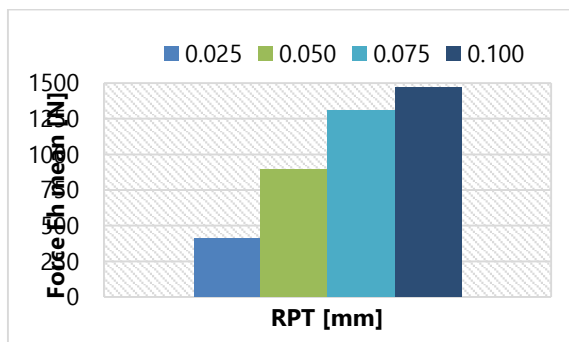
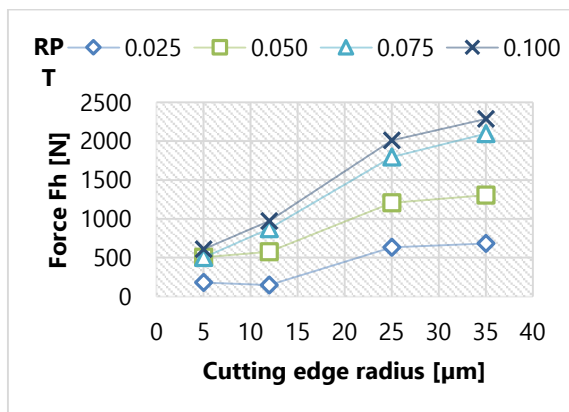


Fig. 15: Behavior of chip forming force

This may be because the contact length has greater dimensional change as the RPT increases. As shown in Figure 16, it can be observed that the magnitude of the contact length is much larger than the contact dimension in the zone of the rounding of the cutting-edge.

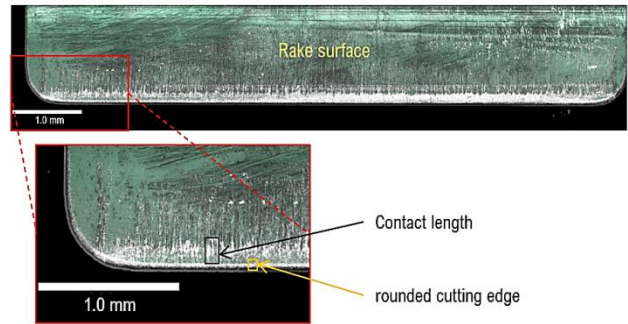


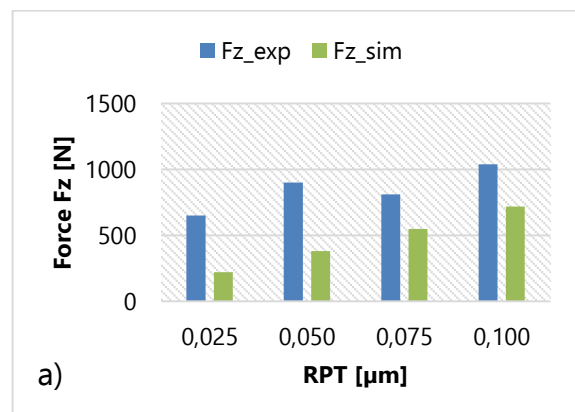
Fig. 16: Contact length between cutting edge-chip and cutting edge rounding for condition: $r_e=15\mu m$, $RPT=25\mu m$

Using equation (4), the average coefficients of friction at the tool-chip interface for machining at different cutting-edge radius were determined and are given in Tab. 4. It is observed that the values are around 1.0. This proves the high friction at the tool-chip interface under the tested conditions. In this case the coefficients are comparable to other studies where friction coefficients of 0.90 were achieved, under the conditions: WC-6%Co cutting insert, corner radius of $r_e = 0.8$ mm and a cutting thickness 3.2 mm, uncut chip thickness $h = 0.1$ mm, rake angle of $\gamma = 6^\circ$ and clearance angle of $\alpha = 5^\circ$ and cutting speed between 10-50 m/min [Alammari et al., 2021].

Tab. 4: Experimentally determined average coefficients of friction m on tool face for orthogonal broaching Inconel 718 with different cutting-edge radius, $V_c = 20$ m/min, rake $\gamma = 7^\circ$.

Cutting edge radius r_e (mm)	5	12	25	35
Coefficient of friction μ	0.99	1.10	1.06	0.95

Figures 17a and 17b compare experimental and simulated results of shear forces in axial (F_z) and normal (F_y) directions, considering an edge radius of 5 micrometers as reference. Although the trends are similar for all conditions evaluated, the numerical values differ. The simulations show relatively low values compared to the experimental data, especially in the normal force F_y . This disparity could be due to geometrical factors or tool wear, aspects that will be investigated in detail in future research. A key aspect to be clarified is why the measured value of the thrust or normal force (F_y) is close to the value of the tangential or shear force (F_z).



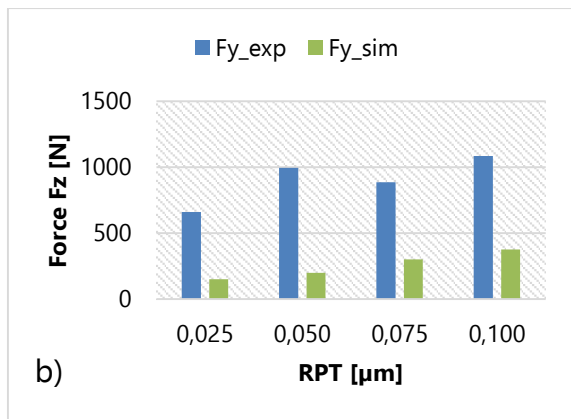


Fig. 17: Comparison of experimental and simulated F_z and F_y force values during the broaching operation of Inconel 718.

4 CONCLUSIONS

The influence of drag-finishing cutting-edge radius on the components of cutting force, specific cutting force and temperature in the orthogonal broaching cutting process of Inconel 718 has been investigated, and the following conclusions are presented.

The experimentally measured cutting force components F_z and F_y increase gradually as the cutting-edge radius changes. Under the tested conditions, the F_z and F_y components have approximately equal values, being a particular characteristic that differs from previous works and that will be sought to find its cause in future works.

According to Albrecht's model the chip forming force F_h reacts more sensitively to a change in cutting-edge radius than the plowing forces F_p . However, the model shows that the contribution of the F_p is important and should not be neglected as it would influence the surface quality.

It was found that the relationship of the increase of r_e with tool temperature is increasing, as is the RPT . The simulation allowed observing that the increase of the edge radius favors the temperature distribution in the profile in a wider way, which implies that it avoids the temperature concentration that would benefit in wear attenuation.

The results in the preparation and characterization of rounded edges obtained a positive K -shape factor of about 1 and a roughness reduction of between 0.05 and 0.12 micrometers. However, their contribution to the increase and reduction of process forces was not quantified. This will be further investigated in subsequent studies, as well as the effect on both the surface quality and the machined surface layer (residual stresses, material microstructure).

ACKNOWLEDGMENTS

This research has been funded by the University group IT1573-22 of the Basque Government, and the grant PID2019-109340RB-I00 funded by MCIN/AEI/10.13039/501100011033 and PDC2021-121792-I00. We also thank H2020 InterQ project for the support in the application of advanced algorithms and some aspects regarding final application. The data models were developed with the help of the project (QUOLINK) Ministerio de Ciencia e Innovación 2021 TED2021-130044B-I00 and by the "European Union NextGenerationEU/PRTR. We thank the Universidad Técnica de Ambato for their support to the research. We thank the Universidad Técnica de Ambato for their support

to the research and the UPV/EHU itself for the financial aid for the pre-doctoral grants PIF 19/96.

REFERENCES

- Alammari Y, Iovkov I, Saelzer J, Wolf T, Biermann D. 2021. Adhesion of Inconel 718 on Uncoated Tungsten Carbide Inserts in Interrupted Orthogonal Machining under MQL. *Procedia CIRP* 103: 194–199.
- Albrecht P. 1960. New Developments in the Theory of the Metal-Cutting Process: Part I. The Ploughing Process in Metal Cutting. *Journal of Engineering for Industry* 82: 348–357.
- Bouzakis KD, Bouzakis E, Kombogiannis S, Makrimalakis S, Skordaris G, Michailidis N, Charalampous P, Paraskevopoulou R, M'Saoubi R, Aurich JC, Barthelmä F, Biermann D, Denkena B, Dimitrov D, Engin S, Karpuschewski B, Klocke F, Özel T, Poulachon G, Rech J, Schulze V, Settineri L, Srivastava A, Wegener K, Uhlmann E, Zeman P. 2014a. Effect of cutting edge preparation of coated tools on their performance in milling various materials. *CIRP J Manuf Sci Technol* 7: 264–273.
- Bouzakis KD, Bouzakis E, Kombogiannis S, Makrimalakis S, Skordaris G, Michailidis N, Charalampous P, Paraskevopoulou R, M'Saoubi R, Aurich JC, Barthelmä F, Biermann D, Denkena B, Dimitrov D, Engin S, Karpuschewski B, Klocke F, Özel T, Poulachon G, Rech J, Schulze V, Settineri L, Srivastava A, Wegener K, Uhlmann E, Zeman P. 2014b. Effect of cutting edge preparation of coated tools on their performance in milling various materials. *CIRP J Manuf Sci Technol* 7: 264–273.
- Cortés C. 2009. Cutting Edge Preparation of Precision Cutting Tools by Applying Micro-abrasive jet machining and brushing. Kassel university press GmbH.
- Denkena B, Köhler J, Ventura CEH. 2013. Customized cutting edge preparation by means of grinding. *Precis Eng* 37: 590–598.
- Drozda Tom, Wick Charles, Benedict JT, Veilleux RF, Bakerjian Ramon, Society of Manufacturing Engineers. 1983. *Tool and Manufacturing Engineers Handbook; Volume I: Machining*. I: 1–1494.
- Engine materials | MTU Aeroport.
- Fabre D, Bonnet C, Rech J, Mabrouki T. 2017. Optimization of surface roughness in broaching. *CIRP J Manuf Sci Technol* 18: 115–127.
- Guo YB, Chou YK. 2004. The determination of ploughing force and its influence on material properties in metal cutting. *J Mater Process Technol* 148: 368–375.
- Klocke F, Vogtel P, Gierlings S, Lung D, Veselovac D. 2013. Broaching of Inconel 718 with cemented carbide. *Production Engineering* 7: 593–600.
- Lv D, Wang Y, Yu X, Chen H, Gao Y. 2022. Analysis of abrasives on cutting edge preparation by drag finishing. *International Journal of Advanced Manufacturing Technology* 119: 3583–3594.
- del Olmo A, López de Lacalle LN, Martínez de Pissón G, Pérez-Salinas C, Ealo JA, Sastoque L, Fernandes MH. 2022. Tool wear monitoring of high-speed broaching process with carbide tools to reduce production errors. *Mech Syst Signal Process* 172: 109003.
- Pérez-Salinas CF, del Olmo A, López de Lacalle LN. 2022. Estimation of Drag Finishing Abrasive Effect for Cutting Edge Preparation in Broaching Tool. *Materials* 2022, Vol. 15, Page 5135 15: 5135.

Sajeev V, Box P, Dhahi A, Vijayaraghavan L, K Rao UR. 2012a. Effect of Tool-Work Deflections on the Shape of a Broached Hole. <http://dx.doi.org/10.7227/IJMEE.28.1.7> 28: 88–92.

Sajeev V, Vijayaraghavan L, Rao URK. 2012b. An Analysis of the Effects of Burnishing in Internal Broaching. <http://dx.doi.org/10.7227/IJMEE.28.2.5> 28: 163–173.

Vogtel P, Klocke F, Puls H, Buchkremer S, Lung D. 2013. Modelling of process forces in broaching Inconel 718. *Procedia CIRP* 8: 409–414.

Wyen CF, Wegener K. 2010. Influence of cutting edge radius on cutting forces in machining titanium. *CIRP Annals* 59: 93–96.

Zhang YL, Chen WY. 2012. Finite Element Modeling of the Broaching Process of Inconel718. *Materials Science Forum* 697–698: 39–43.